CHEMICAL SCIENCES AND TECHNOLOGY

Director's R&D Fund

Nanoscale Photosynthesis, the Photophysics of Neural Cells, and Artificial Sight

E. Greenbaum,[1] T. Kuritz,[1] J. W. Lee,[1] F. W. Larimer,[2] I. Lee,[3] B. Bruce,[4] M. Humayun,[5] and S. Sadda[5]
[1]*Chemical Sciences Division*
[2]*Life Sciences Division Oak Ridge National Laboratory*
[3]*Department of Electrical Engineering*
[4]*Department of Biochemistry/Cell and Molecular Biology The University of Tennessee*
[5]*The Doheny Eye Institute/Keck School of Medicine University of Southern California*

The objective of this work was to impart photoreceptor activity to mammalian cells using the previously determined molecular photovoltaic properties of isolated Photosystem I (PSI) reaction centers. Incubation of WERI-Rb-1 retinoblastoma cells with functional PSI reaction centers that were isolated from spinach leaves and reconstituted into proteoliposomes resulted in a light-induced PSI-dependent increase in intracellular Ca^{2+}. The increase, due to Ca^{2+} uptake, was dependent on the presence of extracellular Ca^{2+} ions. Control experiments in the absence of PSI showed no photoactivity. Application of this hybrid photosynthetic-mammalian system to the problem of artificial sight is discussed.

Introduction

Two triumphs of 20th century photobiological research are elucidation of the molecular mechanisms of vision and photosynthesis. Although both processes are initiated by absorption of visible light, they are chemically and energetically different. In vision, light triggers a thermodynamically downhill reaction that is pre-loaded by dark metabolism. Photon absorption by rhodopsin activates a G-protein cascade leading to cyclic guanosine monophosphate (cGMP) hydrolysis that in turn closes cation-specific channels to generate a nerve signal. A single photon absorbed by a dark-adapted rod closes hundreds of cation-specific channels and leads to a hyperpolarization of about 1 mV that is sensed by the synapse and conveyed to other neurons of the retina.[1] In photosynthesis, on the other hand, absorption of photons by the special reaction center chlorophylls in Photosystems I and II trigger charge separations across the photosynthetic membrane. This charge separation generates a voltage that is the source of Gibbs energy for the thermodynamically uphill reactions of green plant photosynthesis: oxidation of water to molecular oxygen and reduction of atmospheric carbon dioxide to sugars.[2] We have shown that isolated Photosystem I (PSI) reaction centers retain their photovoltaic properties[3–5] and that they are single-molecule diodes.[6] Humayun et al. have demonstrated that the human brain can evoke the perception of light and resolve patterns in individuals who are blind due to macular degeneration or retinitis pigmentosa when retinal tissue is judiciously stimulated by passing current through platinum electrodes.[7,8] In these diseases, which are some of the worldwide leading causes of blindness, neural communication from the eye to the brain is still relatively intact: blindness is caused by loss of the first step in the visual process: photon absorption by rhodopsin followed by activation of the G protein cascade. We report here the insertion of photovoltaically active PSI reaction centers into retinoblastoma cell membranes and observation of light-activated influx of calcium ions into the cells.

The objective of the present studies was to determine if photoreceptor activity could be imparted to mammalian cells by direct insertion of PSI reaction centers into the cellular membranes. The goal of the work was aided by the fact that PSI is an integral membrane protein and the expectation that the mammalian cellular membrane would be a reasonably accommodating environment. The modes of action of PSI reaction centers that are inserted into mammalian cell membranes can be expected to fall into at least two categories. First, the reaction centers may trigger transmembrane photoredox chemistry that alters the intracellular chemical potential and initiates biochemical transformations that do not occur in the absence of light. This is similar to the operation of photosynthetic reaction centers in plants. Second, depending on areal density and proximity to voltage-gated ion channels, PSI might gate the ion channels and/or possibly increase ion permeability by a nonspecific electrical disturbance that increases ion permeability. The photoinduced electric field by PSI in a 5-nm membrane is 10^7–10^8 V·m. Theoretically, PSI reaction centers can depolarize or hyperpolarize a membrane depending on orientation of the electron transport vector of the

photoinduced movement of electrons from donor P700 to the acceptor FAB complex within the reaction center.

Technical Approach

PSI reaction center core complexes were isolated from spinach leaves according to the method of Shiozawa et al.[9] These multimolecular complexes contain 40–45 chlorophyll *a* molecules, β-carotene and cytochromes[9] bound to two PsaA-PsaB heterodimers and up to six other polypeptides.[10,11] Activity of the PSI reaction centers was confirmed by differential optical absorption spectroscopy (810–860 nm)[10] using a Walz Model 103 chlorophyll spectrometer. The sample was comprised of PSI core complexes that were reconstituted into proteoliposome[12] membranes and imaged with the combined techniques of tapping mode atomic force (AFM) and surface scanning probe microscopies (SSPM), illustrated in Fig. 1.[13] The one-to-one correspondence between the AFM and SSPM liposome images is evident. The images were obtained under illumination with a diode laser at 670 nm, near the absorption maximum of chlorophyll *a* (671 nm) in PSI-proteoliposomes. The AFM image of Fig. 1(a) illustrates the gross geometric structure of the PSI-proteoliposome, whereas the electrostatic SSPM image, Fig. 1(b), reveals a finer grained pebble-like structure in the surface potential map, suggesting a close-packing of the PSI reaction centers in the liposome membrane. Photoactivities of the native PSI preparation and the PSI-proteoliposome heterostructure compared favorably with previously reported results of other groups for PSI core particles isolated from spinach,[10] *Synechocystis* sp.,[11,14] and *Spirulina platensis*[15] using a variety of lipids and reconstitution techniques.

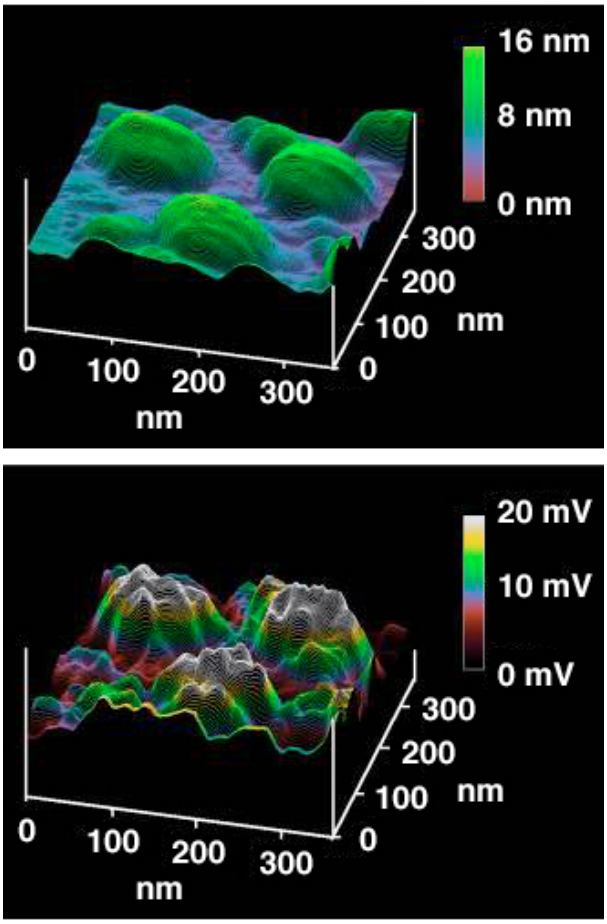

Fig. 1. PSI-proteoliposomes imaged by (a) tapping-mode atomic force (AFM) and (b) scanning surface probe (SSPM) microscopies.

Rigaud et al.[16] pointed out that Triton X-100-mediated reconstitutions resulted in 70–80% orientation of membrane proteins and complexes including reconstitution of lactose transport protein[17] and PSI.[11] Although protein orientation in lipid membranes cannot be predicted from first principles, empirical data demonstrate a dependence of protein orientation on lipid composition of the proteoliposomes. The theory of liposome fusion with biomembranes is far from settled. However, 30-years' experience with liposomes as vectors for drug delivery has resulted in extensive practical experience in the interaction of liposomes with biomembranes and development of numerous liposome-based agents—an increasing number of which are undergoing clinical trials.[18] The liposome preparations reported here used therapeutic model lipid formulations that are known to be incorporated by human and murine cells.[19]

Results and Accomplishments

A retinoblastoma WERI-Rb-1 culture was chosen as the test system for interaction of PSI reaction centers with mammalian cell membranes. WERI-Rb-1 is an undifferentiated, primitive multipotential neuroectoderm culture with the potential to differentiate into neuronal, photoreceptor and glia-like cells making it a reasonable model host with biochemical and immunochemical properties closest to the cells of the optic cup region.[20] Cellular response to light was monitored by visualization of intracellular Ca^{2+} transients.[21] Calcium ion movement is a signal for many physiological events, including photoreception in vision, and is an important factor in cell adaptation to environmental impacts. The culture of human retinoblastoma cells (WERI-Rb-1, ATCC) was anchored to the bottom of the poly-D-lysine precoated slide wells by overnight incubation in the growth medium (RPMI 1640, Invitrogen, Carlsbad, CA). The cells were counted and washed with Hanks saline with or without Ca^{2+} as appropriate, and the proteoliposomes (0.5–2000 ng phosphorus in 500 µl of Hanks saline) were added in different ratios to the cells. All subsequent operations were performed in strict darkness. The slide wells were

incubated for 1 h under growth conditions (37°C, 5% CO_2), the supernatant decanted, and after a wash with Hanks saline were replaced with 500-µl Hanks saline supplemented with 16-µM Fluo-3 AM (Molecular Probes, Eugene, OR) in dimethylsulfoxide (DMSO, Aldrich Chemical, Milwaukee, WI), and 0.02% Pluronic F-127 (Molecular Probes), followed by incubation at 37°C for 2 h. The cells were then washed in the dark with an excess of Hanks saline supplemented with 1 mM ascorbate to ensure that P700 was reduced prior to illumination.

Spectral properties of the system components were selected so that the excitation and emission peaks of the Ca^{2+}-binding dye Fluo-3 did not overlap with the absorption maxima of chlorophyll *a* in PSI particles in the proteoliposomes (Fig. 2). Light-induced Ca^{2+} ion transients were initiated by illumination at 670 nm (1.5 nm bandwidth) using a diode laser (OZ Optics, Ltd., Carp, Ontario). In the presence of an extracellular calcium concentration of 1.26 mM, we observed light-induced intracellular Ca^{2+} fluorescence transients in WERI-Rb-1 cells that were treated with PSI-proteoliposomes containing a concentration of 6.3 ± 2.6 pg [P] per cell. A 3-sec exposure to the 2.5–3.0 µE s^{-1} m^{-2} beam of 670 nm laser light stimulated an increase in intracellular fluorescence in the cells 500 sec after illumination and climbed to a maximum after 1000 sec. The cells then started rupturing and releasing the dye [Fig. 3(a)]. As expected, the dye release led to an abrupt decrease in fluorescence. The time course of calcium increase, bursting of the cells, and abrupt release of the dye illustrates the power and promise of photoreceptor activity by PSI reaction centers. For the WERI-Rb-1 cells chosen for these experiments, cell rupture occurs only at the high PSI-proteoliposome loading for the data of Fig. 3. Lower

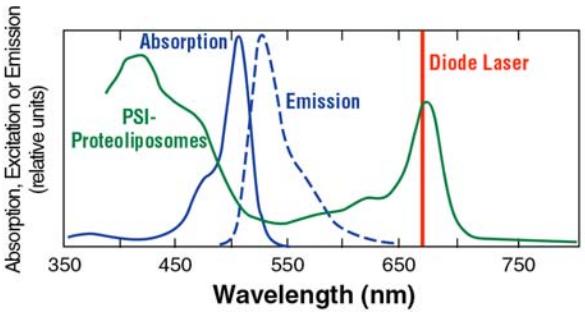

Fig. 2. Absorption, excitation, and emission spectra of the system components. For the Ca^{2+} specific dye Fluo-3, λ_{exc} = 490 nm; λ_{em} = 540 nm (Source: Molecular Probes Catalog, Eugene, Oregon). The green curve is the measured absorption spectrum of PSI proteoliposomes, λ_{abs}^{max} = 671 nm obtained with at Shimadzu Model UV-160 spectrophotometer. The vertical red line at 670 nm is the wavelength emission of the actinic diode laser used to trigger the Ca^{2+} influx (Source: Oz Optics, Ltd., Carp, Ontario). Unlike free chlorophyll in solution, chlorophyll bound to PSI reaction centers emits virtually no fluorescence at room temperature.

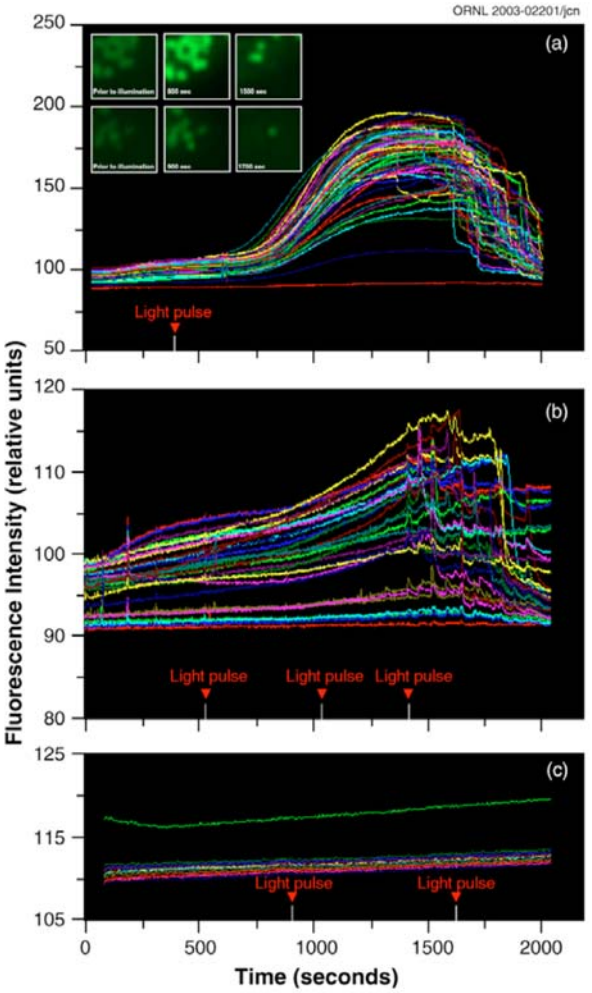

Fig. 3. Response to illumination at 670 nm by PSI-proteoliposome treated WERI-Rb-1 cells in the (a) presence and (b) absence of external Ca^{2+} ions; (c) control experiment with liposome-fused WERI-Rb-1 in the absence of PSI. Inset: Pseudocolor fluorescence image of WERI-Rb-1 cells fused with PSI proteoliposomes at selected time points in the presence (a) and absence (b) of external Ca^{2+} ions. Data were obtained with a Nikon Eclipse TS-100 microscope.

loading does not cause cell death. The reason these are promising results is that elementary electrostatics predicts that charging of the membrane capacitance and the corresponding photogenerated neural voltages can be controlled by appropriate titration of the PSI-proteoliposomes. This conclusion is also supported by the work of Packham et al.,[22] on the areal density-dependent photovoltage of bacterial photosynthetic reaction centers that were incorporated in planar bilayer membranes. Moreover, recent preliminary data indicate that rat retinal progenitor and ganglion cells do not die when treated with proteoliposomes at the concentrations that cause death in WERI-Rb-1.[23] Cell death apparently depends (1) on the nature of the cells; (2) on the dose of PSI-proteoliposomes (data not shown), and (3) on the environment.

The photoinduced increase in intracellular Ca^{2+} occurred simultaneously in all cells. Control experiments [Fig. 3(b)] in the absence of external calcium indicated that cells treated with PSI-proteoliposomes at a concentration of 7.2 ± 4.8 pg [P] per cell also responded to illumination. However, the intensity of fluorescence was about 10-fold less than in the presence of external Ca^{2+}. In the absence of external Ca^{2+}, the light-induced Ca^{2+} spikes in Fig. 3(b) were probably due to the release of intracellular stores. Additional control experiments with liposomes only (no PSI present) at a concentration of 75 pg [P] per a cell [Fig. 3(c)] showed no photoactivity and did not affect cell viability. Figure 4 presents a statistical summary of light-induced fluorescence images in the absence (blue bars, left) and presence of calcium (green bars, right). The bimodal distribution of Fig. 4 demonstrates a 10-fold greater photoinduced fluorescence intensity in the presence of external calcium. Further control experiments with inactive (chlorophyll present, but no photoinduced charge separation) PSI-proteoliposomes and the low-energy fluence used for these experiments exclude photodynamic therapy-like (PDT) effects as the origin of the light-induced Ca^{2+} signal. PDT treatments utilize photon fluences about 1000 times higher than that used in our experiments.[24]

In natural photosynthesis, photon-induced picosecond primary charge separation set in motion the much slower processes of biosynthesis and carbon dioxide assimilation.[25] Similarly, the kinetics of the PSI optically triggered increase in Ca^{2+} concentration in retinoblastoma cells is relatively slow. Yet, that is not surprising since Ca^{2+} is a universal signal messenger and multiple sequential reactions are likely to be set in motion by light-activated PSI. The calcium ion is a universal messenger in eukaryotic signal transducing pathways such as vision, muscle contraction, and many other physiological events.[1] The relatively slow kinetics of extracellular Ca^{2+} uptake (Ca^{2+} channel opening) may be secondary reactions of intracellular biochemistry that are triggered by PSI and the PSI-generated transmembrane voltage in the mammalian cell and not by voltage gating of ion channels directly. This interpretation is consistent with the description of lipid-gated transient receptor potential (TRP) channels.[26] The long-lasting Ca^{2+} influx may be due to the combined effect of TRP with analogs of *Drosophila* postsynaptic density proteins (PDZ), hypothesized to cause a long-persisting signal in retinal neuroepithelium.[27] This suggestion is supported by the findings that the TRP family can respond indirectly to a number of sensory stimuli.

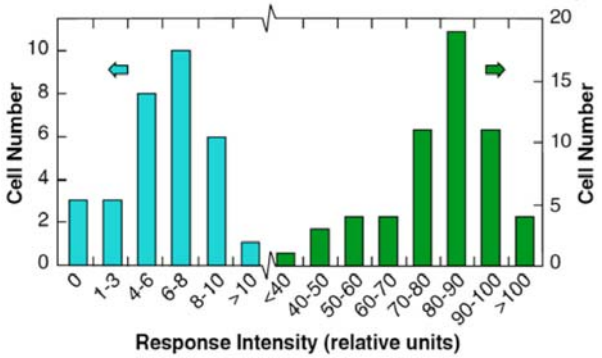

Fig. 4 Statistical distribution of fluorescence images in response to 670-nm illumination in cell populations fused with PSI-proteoliposomes. The bimodal distribution illustrates the effect of the absence (blue bars) and presence (green bars) of externally added calcium. The response was much higher (median intensity of 80–90 brightness units, n = 57) in the cells provided with external Ca^{2+} and lower in the cells devoid of external Ca^{2+} (median intensity of 6–8 brightness units, n = 31). The cells bore a similar load of proteoliposomes (6.34 ± 2.61 pg [P]/cell with external Ca^{2+} vs 7.21 ± 4.8 pg/cell without external Ca^{2+}).

Summary and Conclusions

1. In conclusion, and irrespective of the to-be-determined photobiophysics and photobiochemistry, two biological structures that are evolutionarily separated by at least 2 billion years have been integrated into a functional hybrid photosynthetic-mammalian cell light-induced calcium transport system.
2. The results of our project are of direct benefit to the programmatic mission of DOE's Medical Sciences Division and the NIH's National Eye Institute.
3. This is will be a new FWP in DOE's Medical Sciences Division. Dr. Dean Cole has informed E. Greenbaum that $400K in new funding will be made available to ORNL in FY 2004 to continue the promising results of this successful project.

References

[1]L. Stryer, *Biochemistry*, W. H. Freeman and Company, New York (1995). D. Baylor, *Proc. Natl. Acad. Sci. USA* **93**, 560–565 (1996).

[2]R. Blankenship, *Molecular Mechanisms of Photosynthesis*, Blackwell Science, Oxford, UK, (2002).

[3]I. Lee, B. L. Justus, J. W. Lee, and E. Greenbaum, submitted for publication (2003).

[4]I. Lee, J. W. Lee, A. Stubna, and E. Greenbaum, *J. Phys. Chem. B* **104**, 2439–2443 (2000).

[5]J. F. Millsaps, B. D. Bruce, J. W. Lee, and E. Greenbaum, *Photochem. Photobiol.* **73**, 630–635 (2001).

[6]I. Lee, J. W. Lee, and E. Greenbaum, *Phys. Rev. Letters* **79**, 3294–3297 (1997).

[7]M. S. Humayun, M. Prince, E. J. de Juan, Y. Barron, M. Moskowitz, I. B. Klock, and A. H. Milam, *Invest. Ophthalmol. Vis. Sci.* **40**, 143–148. (1999).

[8]S. Kim, S. Sadda, J. Pearlman, M. Humayun, E. J. de Juan, J. Melia, and W. Green, submitted to *Retina* (2002).

[9]J. A. Shiozawa, R. S. Alberte, and J. P. Thornber, *Arch. Biochem. Biophys.* **165**, 388–397 (1974).

[10]S. Hoshinah and S. Itoh, *Plant Cell Physiol*. **28**, 599–609 (1987); J. Cladera, J.-L. Rigaud, H. Bottin, M. Duñach, *J. Bioenerg. Biomembr.* 28, 503–515 (1996)].

[11]K. Gourovskaya, M. D. Mamedov, I. R. Vassiliev, J. H. Golbeck, and A. Yu. Semenov, *FEBS Lett.* **414**, 193–196 (1997).

[12]The liposomes were prepared by sonicating in buffer (25 mM Tris-HCl, pH 7.8, 10 mM MgCl2, 10 mM NaCl, 1 mM DTT) a mixture of hydrogenated soy phosphatidyl choline and cholesterol (10:1, molar ratio). The proteoliposomes were obtained following solubilization of the liposomes in 1% Triton X-100 according to the methodology of ref. 10 followed by addition of PSI complexes (100–200 times by weight) and reconstitution by gel-chromatography on a Sepharose 6B column equilibrated with the buffer. PSI to lipid ratios were determined by analysis of total phosphorus [C. H. Fiske and Y. Subbarow, *J. Biol. Chem*. **66**, 374–389, (1925)] and by chlorophyll *a* measurement according to MacKinney (*J. Biol. Chem.* **140**, 315–322, 1941) after proteoliposome solubilization in chloroform

[13]The apparent range of liposome diameters was 70–100 nm. The AFM-SSPM technique uses a slender cantilever probe with a slightly blunt apex. It provides accurate voltage measurements but exaggerates lateral dimensions. The theory for this technique has been developed by Jacobs et al. [*J. Appl. Phys.* **84**, 1168–1173 (1998)]. References 4 and 6 provide additional information on our techniques for working with single PSI reaction centers.

[14]J. Cladera, J. L. Rigaud, H. Bottin, and M. Dunach, *J. Bioenerg. Biomembr.* **28**, 503–515 (1996).

[15]J. Kruip, N. V. Karapetyan, I. V. Terekhova, and M. J. Rogner, *J. Biol. Chem*. **274**, 18181–18188 (1999).

[16]J.-L. Rigaud, B. Pitard, and D. Levy, *Biochim Biophys Acta* **1231**, 223–246 (1995).

[17]J. Knol, K. Sjollema, and B. Poolman, *Biochemistry* **37**, 16410–16415 (1998).

[18]R. Blumenthal, M. J. Clague, S. R. Durell, and R. M. Epand, *Chem. Rev.* **103**, 53–69 (2003); K. J. Harrington, K. N. Syrigos, and R. G. Vile, *J. Pharm. Pharmacol.* **54**, 2573–1600 (2002); K. Takiguchi, F. Nomura, T. Inaba, S. Takeda, A. Saitoh, and H. Hotani, *Chem Phys Chem*. **3**, 571–574 (2002). These references provide additional data on the fusion of liposomes with lipid bilayers.

[19]I. Ahmad and T.M. Allen *Cancer Res.* **52**, 4817–4820 (1992); D. E. Lopes de Menezes, L. M. Pilarski, and T. M. Allen, *Cancer Res.* **58**, 3320–3330 (1998).

[20]Retinoblastoma is a childhood intraocular tumor due to uncontrolled growth of undifferentiated retinal photoreceptor (rod) cells [R. C. McFall, T. W. Sery, and M. Makadon, *Cancer Res*. **37**, 1003–1010 [1977)]. M. Campbell and G. J. Chader *Ophth. Paed. Genetics* **9**, 171–199 (1988); G. J. Chader, *Cell Different.* **20**, 209–216 (1987); and A. Kyritsis, G. Joseph, and G. J. Chader, *J. Natl. Cancer Inst.* **73**, 649–654 (1984) reported the ability of retinoblastoma cells to differentiate into cells with characteristics of photoreceptors, conventional neurons, glia and pigment epithelium.

[21]Slide wells with Fluo-3-loaded WERI-Rb-1 cells were fixed in the dark on a thermostated stage (Bionomics BC-1, Technology 2020) and maintained at 37°C throughout the experiment. The dye was excited at 490 nm. Fluo-3 fluorescence emission was collected by an intensified charge coupled device (CCD) (Quantix, Photometrics). We chose a one-second interval for the data acquisition time for digital image collection and a one-second interval during which no data was collected before repeating the cycle. These time intervals allowed acquisition of high-quality images while avoiding excessively large files. Data were collected for up to 4000 sec and processed using Metamorph software (Universal Imaging, West Chester, Pennsylvania). The cells were counted before and after each experiment.

[22]N. K. Packham, P. L. Dutton, and P. Mueller, *Biophys. J.* **37**, 465–473, (1982).

[23]T. Kuritz, G. Qui, E. T. Owens, D.-Y. Wu, S. Sadda, M. Humayun, and E. Greenbaum, unpublished data (2003).

[24]M. L. Agarwal, H. E. Larkin, S. I. A. Zaidi, H. Mukhtar, and N. L. Oleinik, *Cancer Res*. **53**, 5897–5902 (1993).

[25]P. R. Chitnis, *Ann. Rev. Plant Physiol. Plant Mol. Biol.* **52**, 593 (2001). Also reference 2.

[26]C. D. Benham, J. B. Davis, and A. D. Randall. *Neuropharmacol*. **42**, 873–888 (2002); C. Zitt, C. R. Halaszovich, and A. Luckhoff, *Progr Neurobiol* **66**, 243–364 (2002); M. C. Nowycky and A. P. Thomas, *J. Cell Sci.* **115**, 3715–3716 (2002).

[27]S. Tsunoda, J. Sierralta, Y. Sum, R. Bodner, E. Suzuki, A. Becker, M. Socolich, and C. S. Zuker, *Nature* **388**, 243–249 (1997).

Protein Microarray Interactions Readout Using Stepping Sampling Probe/ Electrospray Mass Spectrometry

G.. J. Van Berkel,[1] M. J. Doktycz,[2] G. E. Giles,[3] and S. J. Kennel[2]
[1]*Chemical Sciences Division*
[2]*Life Sciences Division*
[3]*Computational Sciences and Engineering Division*

A rapid, specific, and sensitive method for serial readout of interacting components on protein chip microarrays has been developed. This method makes use of a novel analytical detection concept that requires no extrinsic labeling, which we call stepping sampling probe/electrospray mass spectrometry (SSP/ES-MS). The project consisted of three separate subtasks, viz., development of the probe-readout device, development of affinity capture arrays for readout, and furthering of the "top-down" protein identification of proteins via tandem mass spectrometry. Protein array interactions are read out (i.e., identified) using a miniature sampling probe, connected to an electrospray ion source coupled with a mass spectrometer. The mass spectrometer was used to identify the interacting species on the basis of molecular mass alone or by means of tandem mass spectrometric analysis. Tandem mass spectrometry (MS/MS) of whole proteins in combination with high-resolution accurate mass determinations was shown to generate sequence tags or other diagnostic fragmentation allowing identification of unknown proteins via data-based searching ("top-down" identification). In addition, the developed surface sampling system has demonstrated an unanticipated analytical utility in the read out of thin-layer chromatography (TLC) plates, providing a capability long desired in the analytical chemistry community for on-line TLC/MS. With further experimentation it is anticipated that other important surfaces in biology research, such as protein blotting membranes, will be amenable to analysis with this device.

Introduction

Two-dimensional gel electrophoresis (2-DE) is the most common and powerful platform for monitoring protein expression. Protein "arrays" or "chips" are one potential alternative technology. However, protein microarrays cannot easily exploit the simple labeling and detection (readout) schemes used for DNA microarrays, and thus, detection methods that require no extrinsic labeling are being sought. Mass spectrometry offers a powerful detection option that requires no labeling. While the use of ES-MS for protein-chip-array readout has great potential, it is yet to be demonstrated because of the technical challenge of sampling analytes from a small spot on a sample surface with a liquid flow system in an automated way. The stepping sampling probe/electrospray-mass spectrometry (SSP/ES-MS) approach to reading out protein chip microarrays addresses this challenge. This unique ES-MS surface sampling system combined with our state-of-the-art mass spectrometry instruments is expected to ultimately provide fast, automated, sensitive, and molecular mass and structure-specific means of protein-array readout that cannot be matched by other technologies.

Technical Approach

This two-year project was subdivided into three subtasks that could be independently successful, viz., development of the probe-readout device, development of affinity capture arrays for readout with this probe sampling device, and the furthering of "top-down" protein identification via tandem mass spectrometry. The first six months of the project focused on development of a novel self-aspirating surface sampling probe device. The successful completion and implementation of this device for sampling of surface spotted proteins and thin-layer chromatography (TLC) plates[1] led to submission of a patent application.[2] For the remainder of the project period, emphasis was placed on the other two subtasks, along with application of the probe to the read out of a variety of different surfaces in addition to affinity arrays. The foray examining other surfaces was aimed at exploiting for follow-on funding alternative uses for the probe sampling device.[3]

The affinity capture portion of the project was studied largely off-line from the mass spectrometer using ^{125}I labeled proteins and the corresponding antibodies. In this way protein capture density on the arrays and protein elution efficiency from the arrays with ES-MS-compatible

solvents could be optimized using established detection methodologies. Successful readout of affinity captured proteins, the major milestone of this project, was demonstrated.[4]

Identification of proteins on the basis of the tandem mass spectrometry, top-down approach was studied using two dissociation methods—sustained off-resonance irradiation (SORI) and multipole storage-assisted dissociation (MSAD). Each method was evaluated for generating sequence tag data from intact proteins by FTICR mass spectrometry.

Results and Discussion

Protein Array Preparation. Selective capture of proteins on arrays amenable to readout by the probe sampling device was accomplished by covalently linking antibody to the desired surface and then adding the target protein for specific binding (capture) by the antibody. In the first year of support, FY 2002, this was accomplished for capture of several cytokines using antibodies attached to either glass microscope slides or silicon. Glass slides were masked with Teflon grids leaving 1-mm squares exposed with approximately 1-mm Teflon spacing. Experiments were done with radio-iodinated proteins to quantitate the attachment of the antibody and capture efficiency of the target protein and elution characteristics of the captured protein with solvents compatible with ES-MS. In the second year, approximately six major experiments were done largely in capturing murine gamma interferon, γIFN, with antibody bound to glass slides via a poly-l-Lysine gluteraldehyde bridge. The slides were prepared in parallel, one set with radioactive reagents for quantitative analysis and one for mass spectrometry. Specific capture and elution of radio-labeled γIFN was verified in every experiment. Quantitation of absolute amounts of captured and eluted γIFN varied among the experiments. By use of SDS-PAGE, it was determined that γIFN dissolved in water or normal saline solutions without carrier protein was not stable. Degradation occurred over days to weeks of storage at –20°C with several freeze/thaw cycles. In contrast, protein that had been radio-iodinated and diluted in buffer containing carrier protein (0.5% BSA) was stable and showed consistent integrity as analyzed by SDS-PAGE. In the last several weeks of the project, slides with two specialized ceramic surfaces were tested for their capacity to couple antibody and to capture and subsequently release γIFN. These results indicated that the ceramic slide surface bound about two-fold higher amounts of antibody per unit area than did the glass slide treated in an identical manner. Capture of radio-iodinated γIFN was also about two-fold higher, consistent with the increased amount of capture antibody present. Elution characteristics of the radiolabeled proteins from glass or ceramic were indistinguishable (Table 1). A commercially available aldehyde pre-derivatized ceramic slide performed about the same as the flat glass slide. Two explanations for this result were suggested: (1) the aldehyde derivatization was less dense as deposited by the commercial company than that applied here through the poly-l-Lysine gluteraldehyde bridge, or (2) some loss of reactivity of the aldehdye occurred over the time of shipping and storage of the slides before use.

Table 1. Comparison of glass, ceramic, and aldehyde pre-derivatized ceramic surfaces for antibody-based capture of γ IFN

	Glass	Ceramic	Ceramic prepared
Maximum amt Ab bound,ng/mm^2	33	65	46
Maximum amt γ IFN captured, ng/mm^2	0.35	0.76	0.49
Fraction eluted, %	97	98	92

For the expressed goal of ES-MS analyses, the captured γIFN must be rapidly eluted from the antibody with solvents compatible with ES-MS. In the first year of experiments, we determined that acetonitrile:water:formic acid at 70:30:0.1 volume ratio was the best compromise solvent for elution and spraying. The ability of this solvent to elute captured γIFN was evaluated in each experiment. When elutions were conducted within minutes after removal of the wash solution, greater than 90% of the radioactivity was eluted from all capture surfaces (Fig. 1). The elution occurred with a few second exposure to the solvent. More rapid kinetics could not be evaluated with the radioisotope method. However, if slides with captured γIFN were dried and stored for 18–24 h, the fraction of radioisotope that could be eluted dropped to 50–60%. This phenomenon is difficult to explain at the molecular level but has been observed in other capture systems as well (data not shown).

In summary, efficient capture of cytokines with antibody immobilized on flat surfaces has been demonstrated. The capture is specific, saturable, and

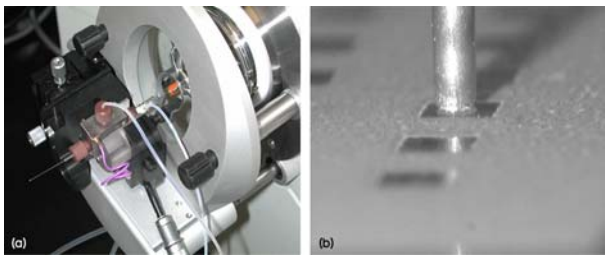

Fig. 1. (a) Surface sampling probe mounted at the atmospheric sampling inlet of a DecaXP Plus ion trap mass spectrometer. (b) View of sampling end of probe sampling from a spot on an affinity array arranged on a glass microscope slide.

related to antibody amounts bound to the capture surface. The captured cytokine can be eluted in nearly quantitative fashion under the right conditions and should be available for detection by ES-MS.

Surface Sampling Probe. Pictures of the surface sampling probe mounted on an ion trap mass spectrometer and the probe sampling from the well of a masked array slide are shown in Fig. 1. Using this probe system, detection capabilities were tested using lysozyme (15153 Da) deposited directly onto a masked glass slide using a peizioelectric spotting device. The amount of protein spotted was varied by increasing the number of droplets deposited in a single location. Each droplet from the peizioelectric spotter was 14 pL in volume and equivalent to 5 fmol of lysozyme per droplet. Two lysozyme spotting experiments were conducted; the first using 60.5, 302.5, 605, 1210, 6050 fmol of lysozyme as the amount spotted; the second using a more dilute series 1, 5, 10, 20, 50, 100 fmol spotted into the wells of the masked slide. Blank spots, with no spotted material, were sampled for both experiments. The first series of spots was sampled 7 times; the second series was sampled 3 times. Examination of the protein signals obtained (+8–+12 charge states) showed that spot to spot reproducibility was good (ca. ±10 %RSD) and linearity in signal with amount spotted up to about 1.2 pmol where signal roll-over occurred. Detection levels of 5 fmol of lysozyme deposited by a peizioelectric spotter were demonstrated.

Figure 2 shows a mass chromatogram acquired from the analysis of surface captured γIFN using the surface sampling ES-MS system. The data shown is the result of the duplicate analyses of 5 different amounts of surface captured protein. The chromatogram is representative of the +10–+19 charge states of this protein. The table in Fig. 2 shows the amounts of γIFN incubated in each masked off area of the slide and the respective amount captured by the antibody as determined by capture efficiency values generated for the array using a parallel radio-labeled assay. The sampling conditions used differed from those used for the surface spotted material in that the operators discretion played a more substantial role in whether or not a sampling event was complete or not. The ES mass spectrum and deconvoluted (zero charge) spectrum in Fig. 3 were obtained by sampling from spot 6 in Fig. 2. This array spot contained about 329 fmol of γIFN. The clearly visible multiply-charged peaks of the protein and the correct mass of the protein determined in the deconvoluted spectrum indicate the successful sampling of a surface captured protein. The controlled experiments did not show a discernable spectrum for γIFN, indicating that our positive result in Fig. 3 was the result of an antibody specific interaction. Spots 7 and 8 which contained more protein gave even better mass spectra. However, when sampling the array spots containing less than 300 fmol of protein, recognizable protein mass spectra were not observed.

Top-Down Protein Identification. Protein samples are often analyzed using a "bottom-up" approach, which typically involves one- or two-dimensional chromatography or electrophoresis, proteolytic digestion of the resulting fractions, and mass spectrometric fingerprinting of component peptides. Tandem mass spectrometry is sometimes performed to provide a more thorough analysis of particularly complex protein mixtures. However, the enzymatic digestion process central to the bottom-up approach not only complicates sample handling but also generates large quantities of data that can be difficult and time-consuming to process. In addition, valuable information about post-translational modifications to the sequence encoded by the genome can be lost because intact protein masses are not determined.

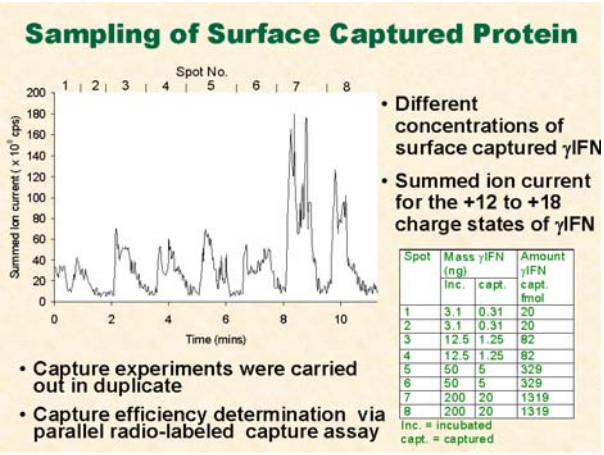

Spot	Mass γIFN (ng) Inc.	capt.	Amount γIFN capt. fmol
1	3.1	0.31	20
2	3.1	0.31	20
3	12.5	1.25	82
4	12.5	1.25	82
5	50	5	329
6	50	5	329
7	200	20	1319
8	200	20	1319

Fig. 2. Mass Chromatogram obtained from the surface sampling of four different amounts of surface captured γIFN.

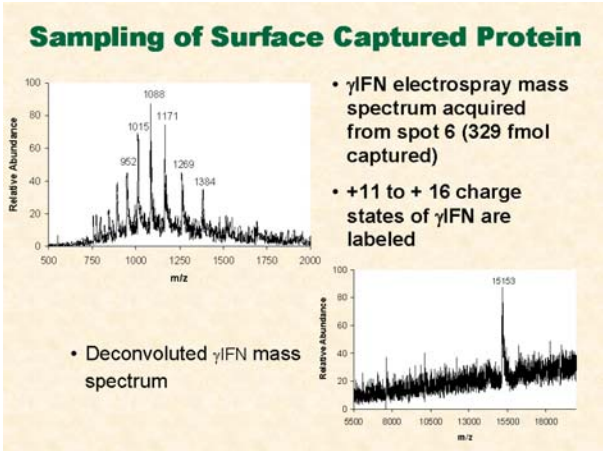

Fig.3. Electrospray mass spectrum and deconvoluted (zero charge) spectrum acquired from sampling of surface captured γIFN from spot 6 in Fig. 2.

The array-readout strategy aims to avoid these time consuming and labor intensive steps in the protein identification.

We explored a "top-down" protein identification strategy that eliminates the digestion process and instead involves direct MS/MS analysis of intact proteins. In this approach, primary sequence information derives exclusively from fragmentation patterns, so robust ion activation techniques are critical. The most effective methods of protein fragmentation include sustained off-resonance irradiation collisionally activated dissociation (SORI-CAD), nozzle-skimmer dissociation (NS), infrared multiphoton dissociation (IRMPD), and electron capture dissociation (ECD).

To date top-down protein analysis has largely been restricted to infusion experiments, in which analyte concentrations are constant. In a variety of applications, such as LCMS or high-throughput protein array analysis techniques under development in this project, analytical signals are transient in nature. Fourier-transform ion cyclotron resonance (FTICR) platforms offer excellent resolution and mass range capabilities in such applications. However, certain dissociation methods available in FTICR instruments, such as SORI and ECD, possess relatively low-duty cycles, and significant portions of a transient signal profile may be poorly sampled. IRMPD offers a relatively high-duty cycle, and was successfully incorporated by Li et al. in the LC-FTMS analysis of a mixture of intact proteins.

IRMPD is not universally available, however, so a role still exists for other methods that allow efficient acquisition of MS/MS data. In multipole storage-assisted dissociation (MSAD), space charge-mediated dissociation occurs in the linear RF-only multipoles commonly used to interface electrospray ionization with FTICR cells. Under certain conditions (extended accumulation times and/or larger dc offset voltages), ion activation and dissociation can be induced during the ion accumulation interval in an inherently high-pressure region of the instrument, so no pump-down periods are required and the overall duty cycle is quite high. Linear ion traps are often used to interface electrospray ionization with FTICR cells, so MSAD can be readily performed on many FTICR instruments with no additional components.

We undertook a systematic comparison of SORI and MSAD for a variety of 8–18 kDa proteins, with particular emphasis on the relative ability of these methods to provide fragmentation information that can be used in database search strategies for the positive identification of the parent proteins. MSAD spectra of intact proteins are influenced by several factors. Data for bovine ubiquitin suggests that because dissociation patterns are charge state dependent, the charge state distribution made available by the ionization conditions may dictate the range of fragment ions that can be generated during the experiment. In addition, conditions of high space charge within the hexapole impair transmission and/or trapping of high m/z species, which can result in loss of important precursor and product ions. And finally, the nonresonant nature of activation in MSAD can provide access to secondary dissociation processes that are not available by SORI. Because of these considerations, the two activation methods do not always provide the same fragmentation information, and MSAD is somewhat less reliable for generating sequence tag data. However, it appears that in general MSAD samples "preferred" cleavage processes (i.e., those occurring at D and P residues) just as well as SORI, which implies that MSAD data may be somewhat more compatible with search algorithms that utilize unprocessed fragment ion masses.

In these experiments the use of MSAD reduced overall analysis time by a factor of two to six over SORI. Other potential advantages of the technique include the fact that it is not necessary to pulse a collision gas into the cell, nor is it necessary to accomplish resonant isolation and activation. However, it remains to be seen whether these advantages can be exploited in the analysis of transient signals. While the nonresonant nature of MSAD could provide rapid, high-throughput analysis of multiple analytes, it also suggests that data interpretation for complex mixtures is potentially problematic. In addition, the charge density dependence of MSAD implies that the degree of fragmentation observed across a transient peak would vary with concentration (i.e., from low to high to low). Judicious choice of MSAD parameters would be necessary to maximize overall dynamic range and sensitivity, and multiplexed scan functions might prove beneficial. Additional experiments will therefore be required to fully characterize/optimize MSAD for applications such as surface sampling or possibly LCMS.

Conclusions

A self-aspirating electrospray probe/emitter coupled with an ion trap mass spectrometer was used to sample and mass analyze proteins deposited onto glass slides or affinity captured on glass slides. Detection levels of 5 fmol of lysozyme deposited by a peizioelectric spotter were demonstrated. From this amount of protein, the correct molecular mass was obtained from the mass spectrum using a commercial deconvolution algorithm. Proof-of-principle sampling of antibody captured proteins was demonstrated for gamma interferron (γ-IFN) using surface immobilized antibody. Results point to increased surface binding capacity and smaller volume probe to limit volumetric dilution and improve ionization efficiency by operating at sub-microliter per minute flow rates. Additional experimental and development work is needed to allow the exploitation of top-down protein identification

of proteins eluted from affinity arrays. While the transients signals proof-of-principle from this study and others in the literature indicate that this possibility may not be far off.

Our demonstrated implementation of this protein array readout technique will lead to an increase in the value of protein arrays in understanding protein-expression monitoring and will establish it as a suitable method to measure murine cytokine levels during a biological reaction. Success will lead to outside interest in development of commercial products that will transcend the current MALDI-MS approach to protein chip array read out. Our success will now also allow us to effectively compete for outside funding from federal agencies including the National Institutes of Health (NIH), the National Cancer Institute, and the Office of Biological and Environmental Research, as well as other sections at DOE, exploiting the current SSP/ES-MS technology for the study of protein expression. With the current data in hand we are in a position to submit a proposal for funding to NIH. Our success will also allow us to pursue funding to develop a refined device, possibly based on the mating of protein microarrays with soon to be commercialized microfabricated arrays of ES nozzles for faster, fully automated serial read out of chip arrays. This tool will meet the call in the DOE Genome To Life program document for revolutionary advance in protein chip arrays and mass spectrometry for the study of protein chemistry. Thus, ORNL's position as a leader in Complex Biological Systems and innovator in characterizing protein biochemistry as part of the DOE Genomes To Life Program will be strengthened.

References

[1]G. J. Van Berkel, A. D. Sanchez, J. M. E. Quirke "Thin-Layer Chromatography and Electrospray Mass Spectrometry Coupled using a Surface Sampling Probe," *Anal. Chem.* **2003***, 74,* 6216–6223.

[2]"Sampling Probe for Microarray Read Out Using Electrospray-Mass Spectrometry," U.S. Patent Application filed April 16, 2002. Inventor: G. J. Van Berkel.

[3]M. J. Ford and G. J. Van Berkel, "Thin-Layer Chromatography and Electrospray Ion Trap Mass Spectrometry Coupled using a Surface Sampling Probe," *Anal. Chem.*, in preparation.

[4]G. J. Van Berkel, M. J. Ford, S. J. Kennel, and M. J. Doktycz, "Electrospray Mass Spectrometry System for Analysis of Proteins Deposited or Captured on Surfaces," *Rapid Commun. Mass Spectrom.*, in preparation.

Reactive Membranes for Clean Coal Technologies

D. W. DePaoli,[1] S. Dai,[2] D. C. Duckworth,[2] J. M. Simonson,[2] C. V. Thompson,[2] M. R. Ally,[3] and R. E. Baltus[4]
[1]*Nuclear Science and Technology Division*
[2]*Chemical Sciences Division*
[3]*Engineering Science and Technology Division*
[4]*Clarkson University*

Coal is the dominant U.S. resource for producing electricity. However, emissions from coal combustion contribute to potential global warming and pose significant environmental threats. This project is aimed at new separations technologies based on ionic liquids that would allow sustainable use of coal resources. Because they have tunable chemical properties, a wide stable temperature range, relatively benign character, and essentially zero vapor pressure, ionic liquids show great promise as reaction and separations media. This project has explored the feasibility of ionic-liquid-based separations technologies for removal of carbon dioxide and mercury from flue gas through laboratory experimentation, thermodynamic modeling, and preliminary economic evaluation. Ionic liquids having significantly higher solubility of carbon dioxide than those previously reported in the literature were synthesized; preliminary analysis indicates that, with further development, absorption or membrane processes based on these liquids may be competitive with existing technologies. An ionic liquid with high affinity for elemental mercury was discovered and shown to be effective for removal of mercury from the gas phase; to enable practical application, further research is needed to determine effective means of regeneration. This project is expected to advance DOE's energy-security mission by providing initial data on ionic-liquid-based separations technologies for clean-energy processes.

Technical Approach

Currently, approximately 50% of the country's electricity is generated from coal, and it remains a vital raw material for the United States and world economy. However, emissions from coal power—including greenhouse gases, acid gases, and mercury—pose significant environmental threats.[1] Because carbon dioxide (CO_2) is generally recognized as the major greenhouse gas leading to global warming, there has been increasing interest in the development of economically viable technologies for the removal of CO_2 from flue gas streams. The President's Energy Plan identifies emission of mercury as a major obstacle to clean coal power. The Environmental Protection Agency is expected to release new standards for power-plant mercury emissions by December 2004. The regulations will aim for a 90% reduction in the 43 tons of mercury released annually by coal-fired power plants.[2] With the current threat of mercury contamination, and the pending EPA regulations, new, cost-effective technologies for mercury removal are sought.

This project was aimed at determining the technical feasibility of creating "designer" ionic liquids for clean-energy processes, such as the selective removal of carbon dioxide and mercury from gas streams produced by coal combustion. Ionic liquids are relatively new compounds that have received increased attention in recent years as "green" designer solvents that may potentially replace many conventional volatile organic solvents in reaction and separation processes.[3] These unique compounds are organic salts that are liquid over a wide range of temperatures near and at room temperature. Ionic liquids have no measurable vapor pressure; hence, there has been considerable interest in using them in place of volatile organic solvents that can emit problematic vapors.

The most commonly investigated room-temperature ionic liquids have an alkyl-substituted imidazolium salt as the cation. The imidazolium-based salts are relatively easy to synthesize and have physical properties that make them attractive for many chemical processes. The generally accepted acronym for the alkyl-substituted methyl imidazolium cations used in these studies is C_nmim^+, where *n* is the number of carbon atoms on the alkyl side chain. Common anions used in ionic liquids include bis[trifluoromethylsulfonyl] amide (Tf_2N^-), hexafluorophosphate (PF_6^-), tetrafluoroborate (BF_4^-), and ethyl sulfate ($EtSO_4^-$), although ionic liquids with a variety of other anions have also been synthesized.

This project employed ORNL capabilities in synthetic chemistry, thermodynamics, analytical chemistry, and engineering research to investigate the feasibility of gas separations using ionic liquids. Elements of the work included (1) synthesis and screening of ionic liquids for

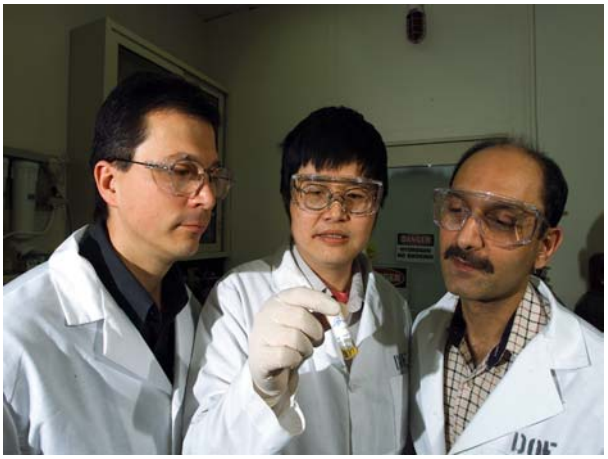

Fig. 1. Researchers examine a vial of ionic liquid. This ionic liquid was tested to determine its effectiveness in removing carbon dioxide from a mixture of gases.

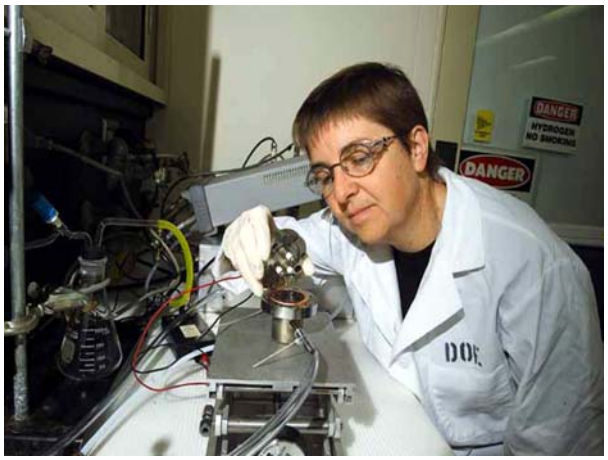

Fig. 2. A quartz-crystal microbalance test cell, which is used to screen different ionic liquids for their ability to absorb CO_2 from a gas mixture, is assembled. The ionic liquid is coated on a piezoelectric quartz crystal that is electronically excited into resonance. As the ionic-liquid-coated quartz is exposed to varying concentrations of CO_2, the resonance frequency changes because of the uptake and release of dissolved CO_2. These frequency changes are interpreted in terms of the effectiveness of the liquid in removing CO_2.

efficient separations, (2) predicting and verifying chemical and physical properties of ionic liquids, (3) development of ionic-liquid-based processes for removal of target compounds, and (4) preliminary technical and economic evaluation of novel processes.

Results and Accomplishments

Fourteen ionic liquids were synthesized, and their relative affinities for the target compounds (carbon dioxide and/or mercury) were assessed.

Carbon Dioxide Separation

The solubility of CO_2 in a series of imidazolium-based room-temperature ionic liquids was determined by a technique developed that employs a quartz crystal microbalance (QCM). Results were reported[4] in terms of Henry's Law constants, as shown in Table 1. A smaller value of Henry's Law constant indicates greater solubility of the gas in the liquid. For comparison, the Henry's Law constants for CO_2 are 1670 in water and 100 in toluene. The measured values of Henry's Law constant are in good agreement with published data for similar compounds that were obtained by other means,[5] supporting the viability of the QCM technique. A comparison of the results in Table 1 helps in understanding the role of chemical structure on the separation capabilities of these materials. Notable among the results is a significantly greater measured CO_2 solubility in an ionic liquid having a fluorine-substituted cation as compared to the corresponding ionic liquid with a non-fluorinated cation. The Henry's constant of 4.5 for that liquid (C_8F_{13}mimTf_2N) is several times lower than the smallest value reported in the literature for ionic liquids that do not undergo a chemical reaction with CO_2. This finding is important both for practical reasons in discovering better solvents for carbon dioxide and for fundamental science, since researchers at other leading institutions have reported that CO_2 solubility is primarily determined by the anion of the ionic liquid. The presence of water vapor was determined to have a minor effect on CO_2 solubility in hydrophobic ionic liquids, which is of practical importance given the water vapor present in flue gas.

Table 1. Henry's law constants for CO_2 in ionic liquids

Ionic liquid	H_{CO2} (bar)
C_3mim Tf_2N	37 ± 7
C_3mim PF_6	52 ± 5
C_4mim Tf_2N	37 ± 3
C_6mim Tf_2N	35 ± 5
C_8mim Tf_2N	30 ± 1
C_8mim Tf_2N with 20% relative humidity	30 ± 2
C_8mim Tf_2N with 40% relative humidity	27 ± 4
C_8F_{13}mim Tf_2N	4.5 ± 1
58 mol% C_8mim Tf_2N/42 mol% C_8F_{13}mim Tf_2N	15 ± 1
1,4-dibutyl-3-phenyl-imidazolium Tf_2N	63 ± 7
1-butyl-3-phenyl-imidazolium Tf_2N	180 ± 17

An irregular-ionic-lattice model (IILM) was developed to provide a means to predict the vapor pressures and solubility of carbon dioxide dissolved in ionic liquids throughout a range of pressures and

temperatures.There are only two parameters in this thermodynamic model and they were shown to be independent of an arbitrarily chosen reference state. Model predictions were compared with good agreement against published experimental data[5] for C_3mim PF_6 and C_8mim BF_4. The model may be useful in predicting CO_2 solubility at temperatures and pressures where experimental data is unknown. This is a significant finding; two papers on the subject were submitted to peer-reviewed journals.[6,7]

Laboratory-scale membrane tests systems were set up and operated to measure the flux and selectivity of gas transport through supported ionic-liquid membranes. The pores of anodic alumina membranes (Whatman, 47-mm diameter, 0.02-µm pore size and 60-µm thickness) were saturated with ionic liquids to create the membranes for the experiments. Transport rates of gases were measured for several ionic liquids using single- and mixed-gas feeds. Considerable selectivity of carbon dioxide over nitrogen transport through the membranes was measured, as shown in Table 2. The greater permeance of CO_2 through membranes containing C_4mimTf_2N compared to C_8F_{13}mimTf_2N—despite the significantly greater CO_2 solubility in the latter—can be explained by recognizing that the permeance of a supported liquid membrane to a particular species reflects both the solubility and the diffusivity of the species in the liquid. C_8F_{13}mimTf_2N was noticeably more viscous than C_4mimTf_2N. This higher viscosity is consistent with lower diffusivity, which apparently counters the favorable thermodynamics for this ionic liquid. These results point to the importance of addressing transport properties as well as thermodynamic equilibria in development of ionic liquids for separation applications.

Using the measured values of CO_2 solubility in ionic liquids and the measured membrane transport characteristics, a preliminary economic analysis of a separation process based on supported ionic liquid membranes was performed.[8] The cost of employing this membrane-based separation process for removal of carbon dioxide in the effluent of a coal-fired power plant was estimated and compared with a published analysis for a conventional amine scrubbing process.[9] The comparison indicates that, with continued technology development, an ionic liquid membrane process may potentially be economically competitive with the project cost of $33/mt CO_2 emission avoided for amine scrubbing.[9] In addition, an estimate of the cost of replacing the solvent in an amine scrubber with an ionic liquid also indicates that an ionic-liquid based process could potentially be competitive. This preliminary evaluation suggests that further investigation of ionic liquid processes for carbon dioxide capture is warranted.

Table 2. Measured CO_2 and N_2 permeance in supported ionic liquid membranes

Supported ionic liquid	Gas	Permeance (mol bar^{-1} cm^{-2} sec^{-1})	Selectivity
C_4mimTf_2N	CO_2	4.0×10^{-9}	127
	N_2	3.2×10^{-11}	
C_8F_{13}mimTf_2N	CO_2	1.5×10^{-9}	72
	N_2	2.1×10^{-11}	

Mercury Capture

Three ionic liquids were synthesized with the goal of imparting high affinity for mercury. These "task-specific" liquids were screened by conducting experiments in which gas streams containing trace levels of redox-generated metallic mercury vapors were passed by membranes coated with ionic liquid. A time-of-flight mass spectrometer was used to detect changes in the mercury concentration in the outlet stream from the membrane cell as mercury was removed by the ionic liquid. Two of the ionic liquids tested removed less than 30% of the mercury in the gas stream, while the third exhibited very high affinity for mercury. Greater than 99.9% mercury removal persisted for the duration of the tests, which lasted over 2 h.

Further experiments focused on the ionic liquid with high mercury affinity, and they were aimed at obtaining information needed for preliminary evaluation of the liquid for practical applications. The mercury capacity of the ionic liquid was measured to be 4.4 mg mercury per g of ionic liquid by analyzing the mercury content of a sample of ionic liquid that was equilibrated with mercury-saturated air at 26°C. Column testing was conducted to observe mercury removal performance in a flowing gas stream. Air containing a given concentration of elemental mercury vapor was passed through filters impregnated with a small amount ionic liquid, and samples of the inlet and outlet gases were analyzed. Excellent mercury removal performance was measured, as shown in the representative results of Fig. 3. In that test, a very small amount (12 mg) of ionic liquid was coated onto the surfaces of a porous filter (Millipore AP prefilter AP25-02500). Mercury-laden gas was passed through the filter at a relatively high flow rate (150 mL/min) that resulted in a contact time of the gas with the ionic liquid films of less than one second. Essentially complete mercury removal was achieved during the first 43 h of the experiment at an inlet concentration of 45 ng/L, and good removal persisted for many hours after the inlet concentration was increased by a factor of 23. The breakthrough from the column was consistent with the estimated mercury capacity of the ionic liquid. These positive results indicate rapid mass transfer performance of the ionic liquid and support its further investigation for gas-phase separations.

Further experiments were conducted to explore practical means for regeneration of the solvent for mercury

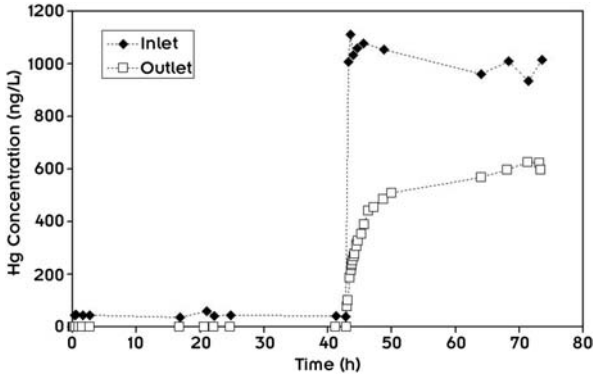

Fig. 3. Excellent results were obtained in column testing of mercury removal from a gas stream using an ionic liquid. Essentially complete mercury removal was achieved during the first 43 h of this test with 12 mg of ionic liquid, indicating significant mercury capacity and rapid mass transfer. Good removal persisted for many hours after the inlet concentration was increased by a factor of 23.

recovery and solvent reuse. Thermogravimetric analyses of both neat and mercury-loaded ionic liquid indicated that mercury was retained in the ionic liquid above the temperature at which the ionic liquid begins to thermally decompose. While those results indicate that thermal regeneration is not feasible, they underscore the strong binding of the mercury in the ionic liquid and indicate the capability for mercury capture at elevated temperatures.

Summary and Conclusions

This work has contributed to DOE's energy-security mission by providing positive information on the feasibility of ionic-liquid-based separations that could be used in future clean-energy processes. Ionic liquids were synthesized that were shown to have high affinity for carbon dioxide and mercury, target compounds for capture from exhaust gases from fossil-fuel combustion. Preliminary technical and economic evaluations indicate that further investigation of these ionic liquids is warranted. This project has also contributed to DOE's science mission by providing basic information on the chemical and physical properties of new ionic liquids and will help guide synthesis and application of these "solvents of the 21st century."

Products of this project included four research papers submitted to peer-reviewed journals, a master's thesis,[8] and three presentations at national technical meetings. An invention disclosure is in preparation on an ionic liquid for gas-phase mercury removal. In addition to ORNL staff from three divisions, the project supported efforts by a visiting professor on sabbatical (R. E. Baltus), a graduate student from the University of Tennessee (B. H. Culbertson), and an undergraduate summer student from Texas A&M University (C. Harris).

References:

[1]C. Krause, "Clean Coal Power Technologies," *Oak Ridge National Laboratory Review*, Vol. 35, No. 2, 2002. <http://www.ornl.gov/info/ornlreviewvol35/_2_02/clean_coal.shtml>.

[2]*Fact Sheet: EPA to Regulate Mercury and Other Air Toxics Emissions from Coal- and Oil-Fired Power Plants*, U.S. Environmental Protection Agency, Washington DC (2000). [Online]. Available: http://www.epa.gov/ttn/oarpg/t3/fact_sheets/fs_util.pdf.

[3]R. D. Rogers and K. R. Seddon, "Ionic liquids—Solvents of the future?" *Science* **302**, 792–793 (October 2003).

[4]R. E. Baltus, B. H. Culbertson, S. Dai, H. Luo, and D. W. DePaoli, "The low-pressure solubility of carbon dioxide in room-temperature ionic liquids measured with a quartz crystal microbalance," *J. Phys. Chem. B,* in press (2003).

[5]J. L. Anthony, E. J. Maginn, and J. F. Brennecke, "Solubilities and thermodynamic properties of gases in the ionic liquid 1-*n*-butyl-3-methylimidazolium hexafluorophosphate," *J. Phys. Chem. B* **2002**, 106, 7315.

[6]M. R. Ally, J. Braunstein, S. Dai, J. M. Simonson, and D. W. DePaoli, "Carbon dioxide gas solubility in ionic liquid 1-n-octyl-3-methylimidazolium hexafluorophosphate [C8mim][PF6] from the irregular ionic lattice model," submitted to *J. Chem. Eng. Data* (2003).

[7]M. R. Ally, J. Braunstein, R. E. Baltus, S. Dai, D. W. DePaoli, and J. M. Simonson, "Irregular ionic lattice model for gas solubilities in ionic liquids," submitted to *Ind. Eng. Chem. Res.* (2003).

[8]B. H. Culbertson, R. E. Baltus, H. Luo, S. Dai, and D. W. DePaoli, "Examination of the potential of room-temperature ionic liquids for gas separations," submitted to *Sep. Sci. Technol.* (2003).

[9]D. R. Simbeck. "CO_2 mitigation economics for existing coal-fired power plants," U.S. Department of Energy National Energy Technology Laboratory First National Conference on Carbon Sequestration, Washington, D.C., May 14–17, 2001.

[10]B. H. Culbertson "CO_2 Separation and Fuel Desulfurization Involving Room-Temperature Ionic Liquids," M.S. Thesis, University of Tennessee, Knoxville, Tennessee, May 2003.

Structure and Dynamics of Fluids in Confined Geometries

D. R. Cole,[1] J. M. Simonson,[1] M. Gruszkiewicz,[1] A. A. Chialvo,[1] G. D. Wignall,[2] Y. B. Melnichenko,[2] J. S. Lin,[2] G. W. Lynn,[2] B. Gu,[3] K. L. More,[4] T. D. Buchell,[5] P. T. Cummings,[5] Y. Leng,[5] K. E. Gubbins,[6] A. Striolo,[6] W. T. Cooper,[7] M. Schilling,[7] and A. Habenschuss[1]

[1] *Chemical Sciences Division*
[2] *Condensed Matter Sciences Division*
[3] *Environmental Sciences Division*
[4] *Metals and Ceramics Division*
[5] *Department of Chemical Engineering, Vanderbilt University, Nashville*
[6] *Department of Chemical Engineering, North Carolina State University, Raleigh*
[7] *Department of Chemistry and Biochemistry, Florida State University, Tallahassee*

Fluids including hydrocarbons, aqueous solutions, and gaseous species (e.g., CO_2, CH_4) can occupy the pores or fractures within solid matrices. The size, distribution, and connectivity of these confined geometries, the chemistry of the solid, and the chemistry of the fluids and their physical properties collectively dictate how fluids migrate into and through these micro- and nano-environments, wet and ultimately react with the solid surfaces. Our multidisciplinary approach combined scattering experiments, simulations, and thermodynamic measurements to quantitatively assess molecular properties of fluids confined to well-characterized porous media, subjected to a wide range of experimental conditions. Results were obtained in four distinct, interrelated areas. Scanning electron microscopy (SEM), transmission electron microscopy (TEM), X-ray diffraction (XRD), and small-angle X-ray and neutron scattering (SAXS, SANS) have been used to characterize a number of porous silicas, carbon fiber monoliths, zeolites, and clays, prior to interaction with fluids. Water adsorption/desoprtion isotherms have been determined on these materials from 105 to 200°C. Fourier transform infrared (FTIR), nuclear magnetic resonance (NMR), quasi-elastic neutron scattering (QENS), and SANS have been used to investigate structural and dynamic features of fluid-matrix interactions. Molecular dynamics (MD) simulations have focused on the behavior of water in carbon slit pores, carbon nanotubes, and mica. These studies are providing an understanding at the molecular level of how intrinsically different fluids behave in confined geometries, compared to bulk systems.

Introduction

The porosity (void) volumes within the solids span wide length scales including micro-, meso-, and macroporous regimes (d/Å < 20, 20 < d/Å < 500, and d/Å > 500, respectively, as defined by IUPAC). A number of factors dictate how fluids, and with them reactants and products of intra-pore transformations, migrate into and through these nano-environments, wet and ultimately adsorb and react with the solid surfaces. These include the size, shape, distribution, and interconnectivity of these confined geometries, the chemistry of the solid, and the chemistry of the fluids and their physical properties. The dynamical behavior of fluids and gases contained within solids is controlled by processes occurring at the interface between the various phases (e.g., water-water, water-solute, water-solid, solute-solid, etc.), as well as the rates of supply and removal of mobile constituents. The richness and complexity of fluid behavior (e.g., phase transitions, molecular orientation and relaxation, diffusion, adsorption, wetting, capillary condensation, etc.) in confined geometries only underscores the need to adopt a multidisciplinary approach when trying to quantify this behavior regardless of the fluid type or nature of the porous medium. If properly calibrated and scaled, an atomistic or molecular understanding of fluid-solid interaction may provide quantitative insight into the behavior of systems at the macroscopic level. The overall objective of our work was to show that the fundamental molecular properties and behavior of fluids confined to restricted geometries can be understood through the combination of detailed experimental studies with theory and molecular-level simulation, and that this understanding can open new avenues for future improvements in processes and systems in natural and technological environments relevant to DOE.

Technical Approach

In order to assess key features of the fluid-matrix interaction under confinement at the nanoscale, a multidisciplinary approach was taken that addressed the

following areas: (a) characterization of the physical nature (e.g., size, shape, fractal geometry, etc.) of the pores using various types of microscopy (SEM; TEM), scattering (SAXS; SANS), XRD, and gas sorption methods; (b) determination of the thermodynamic properties of water in confined geometries using the isopiestic method over a wide ranges of temperature and pressure; (c) determination of the local short-duration dynamics and longer-scale hindered motion of water, CO_2 and hydrocarbons through use of complementary techniques including neutron scattering, NMR, and FTIR spectroscopy, as a function of pressure and temperature; (d) application, refinement, and, where necessary, development of molecular-based simulations methods that describe the properties and structure of confined fluids. Selected aspects of these activities are highlighted below.

Considerable effort was expended to obtain a set of porous materials exhibiting varying porosity, pore sizes, shapes, distribution, and chemistries. Because many of these materials were used in more than one kind of study, multiple-gram quantities of each material were obtained so they could be shared among the investigators. Table 1 summaries the porous solids used in experiments and/or simulations, and some of their characteristics. The solids we selected for study had many of the following characteristics: (a) sparingly soluble at the pressure-temperature-fluid composition conditions of the experiments; (b) suitable for detailed characterization of pore features such as size, shape, distribution, roughness, etc.; (c) susceptible to chemical manipulation from hydrophobic to hydrophilic by chemical pretreatments; and (d) limited crystallinity to minimize the impact on small-angle scattering. In addition to the more conventional methods typically used to characterize porous matrices (SEM, TEM), we used a number of scattering and spectroscopic techniques. Many of these materials were either machined or synthesized into specific shapes and sizes in order to accommodate the various sample or environmental chambers used in our experiments. Vycor 7930 pore glass, machined into various shapes (e.g., elongate cylinders, plates) and polished, was cleaned initially by boiling for several hours in H_2O_2. Silica aerogels (densities of 0.01, 0.1 and 0.2 g/cm^3) were synthesized from different mixtures of TMOS and methanol, and supercritically dried. All silica materials were heat treated to drive off unwanted organics (e.g., SiO-CH_3 groups) by slowly heating over a several-hour period to 600°C in air, followed by slow cooling back to room temperature. Carbon fiber monoliths with varying porosities and surface areas were synthesized here at ORNL. Natural Ca-zeolite was hydrothermally pretreated and converted to Na or Na-K zeolites. The pillared aluminous-rich clay (montmorillonite) was obtained from Fluka (Sigma Aldrich; Lot 381121/1 13301). Prior to any characterization or experimentation, these materials were preheated to 100–110°C under vacuum to drive off adsorbed water.

Because of its ubiquitous presence in both natural and industrial settings, water in its bulk liquid or solid forms has been the subject of numerous theoretical and experimental investigations. As such, we elected to focus much of our effort in this project on the behavior of water in confined geometries. In addition to water, we also explored the influence of confinement in porous silica glass on the behavior of aqueous electrolytes (LiCl, $CaCl_2$, $NdCl_3$). A select number of non-aqueous systems (e.g., chloroform, aniline, and CO_2 were investigated using NMR, FTIR, and SANS, respectively).

Table 1. Porous solids used in experiments and/or modeling

Solid	Surface	Pore shapes	Pore widths (nm)
Porous glass	O, Si	Cylinder	2–8
Silica sol-gels	O,Si	Cylinder	2.5–20
Silica aerogel	O, Si	Irreg. cyl.	6–7
Activated C fibers	C (O, H)	Varied	0.4–1.0
C nanotubes[a]	C (O, H)	Cylinder	1.0–1.6
Na-K Zeolites	K, Na, Si, Al, O	Cylinder, cage	0.3–0.8
Montmorillonite	Na, Si, Al, O	Slit, pillars	0.5–0.8
Muscovite (2M1)[a]	K, Si, Al, O	Slit	0.6–1.0

[a]Solids investigated in modeling studies only.

Results and Accomplishments

Physical Characterization of solids is a crucial step that sets the stage for how variations in pore size, roughness, distribution, connectivity, composition (hydrophobic versus hydrophilic), surface charge, and structure (i.e., crystalline versus amorphous) influence molecular behavior of confined fluids. In addition to the more conventional methods typically used to characterize porous matrices (gas sorption isotherms, SEM, TEM), we used a number of scattering and spectroscopic techniques. While not yielding direct imaging information, scattering and diffraction experiments can provide global statistical information about interfaces (e.g., total porosity, pore surface area, pore length scale, skeletal density, fractality) over an enormous range of length scales (Å to mm), represented by reciprocal or Q-space (where $Q = 4\pi\lambda^{-1}\sin\theta$ is the momentum transfer, 2θ is the angle of scattering, and λ is the wavelength). The scattering intensity, $I(Q)$, is measured as a function of momentum transfer, and exploits the difference in scattering power (contrast) between the solid matrix, and air or fluid occupying the pore space. An example of results from small-angle neutron scattering (SANS) is shown in Fig. 1 for three different porous silica sol-gel glasses. This plot reveals that the correlation peaks (vertical arrows) shift to successively longer distances, which is

indicative of variations in the dehydration process designed to produce the different pore sizes. The glass with 75-Å pores yields the minimal excess scattering in the small-angle region, which makes it better suited for studying the influence of confinement on liquid-gas critical behavior. For the most part, the disordered porous-silica glasses have rather smooth pores that are uniformly distributed throughout the solid. The porous carbons have more wide-ranging pore sizes and exhibit varying degrees of crystallinity, depending on the temperature of burn-off and the duration used to activate the solid.

The Sorption Capacity of a porous or fractured solid matrix depends on the total exposed solid surface area, the shape and size distribution of voids in the matrix, and the nature of the interaction between fluid molecules and the solid surface, and between the molecules themselves. The competition between liquid-solid and liquid-liquid interactions leads to monolayer and cluster formation at low pressure and capillary condensation at high pressures. In order to understand these effects in a fluid with strong intermolecular interactions, adsorption/desorption isotherms of water were measured for 15 solid samples (e.g., porous silicas, carbon fiber monoliths, zeolites, pillared clay) at 105, 150, and 200°C from vacuum to saturated vapor pressure in an isopiestic apparatus. This apparatus is unique in its capability for precise weighing of samples at elevated temperature and pressure between vacuum and 4 MPa. This gravimetric method, in contrast to the more common volumetric techniques, allows for continuous monitoring of the changes of the adsorbent itself due to degassing, oxidation, or decomposition.

Figure 2 shows representative water sorption results at 105°C from vacuum to saturated vapor pressure (0.121 MPa) for several of the porous solids. At low pressure the isotherms reflect competition between liquid-solid and liquid-liquid interactions (forming the monolayer and subsequent clusters or layers; pore filling). The behavior at higher pressures reflects the impact pore size and structure have on capillary condensation and possible hysteresis. Both zeolites exhibit very steep isotherms at low pressure followed by relatively flat trends at moderate to high pressures. This behavior is indicative of strong water-solid intermolecular interaction dominated by mono-layering. The porous carbon and silica glass have rather flat slopes at low pressure followed by steep trajectories indicating weak water-solid interaction and capillary-like pore filling. The montmorillonite exhibits a steady increase in water uptake, suggestive of multi-layering characteristic of dipolar electrostatic interaction. In general, an increase in temperature produces a narrowing of the hysteresis loops, a decrease in the magnitude of water uptake, but essentially unaltered shapes of the sorption curves. One exception was the behavior of the clay, wherein the isotherms exhibited a different shape at each temperature due to a repeated sequence of desorption and adsorption of relatively weakly attached H_2O ligands and OH^- groups followed by physical adsorption. Results such as these can form the basis of testing various MD simulation schemes.

Vibrational Behavior and Molecular Motion of water and nonaqueous solutions (e.g., aniline, chloroform) in confined geometries have been assessed with FTIR and NMR spectroscopy, respectively. The FTIR data indicate that once water molecules are sorbed or "confined" within the pillared Al-montmorillonite, their structural arrangements became more ordered as demonstrated by the shifts in the symmetrical and asymmetrical stretching vibration and deformation of the water molecules. Free water molecules (for fully hydrated Al-clay) exhibited O-H stretching-deformation at ~1652 cm^{-1}, whereas water molecules in confined micropores showed crystalline-like structure with O-H stretching deformation shifted to lower wave number at ~1630 cm^{-1}. This blue shift in wave number (~22 cm^{-1}) is indicative of a relatively high energy required for the O-H stretch deformation because of confinement of water molecules.

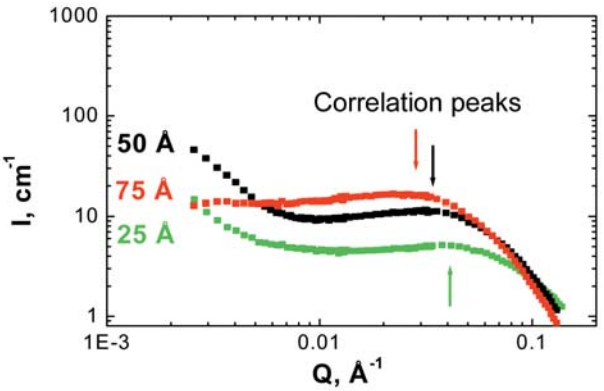

Fig. 1. SANS results from various silica sol-gel glasses having different average pore sizes.

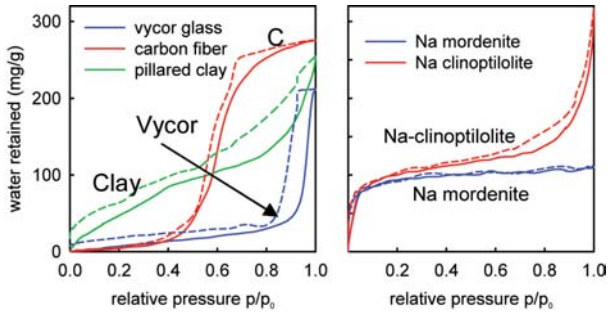

Fig. 2. Adsorption (solid) and desorption (dashed) isotherms of water measured for a variety of porous solids at 105°C.

Relaxation Parameters derived from NMR measurements were used to characterize the tertiary structure of soil organic matter (SOM) and the molecular motion of water (and chloroform) confined to pores in soil and Vycor silica glass, respectively. In the case of water, NMR data indicate that at pore filling levels below ~30%, water is highly mobile, probably existing as surface-bound vapor and not as a water cluster with liquid-like properties. Beyond 30% filling, water behaves an isotropic liquid and exhibits diffusion coefficients characteristic of bulk water. Chloroform, however, appears to behave differently, with restricted motion (i.e., decreasing diffusion coefficients) extending well beyond the 30% pore volume filling exhibited by water.

Phase Transitions can be significantly modified by confinement and disorder. The liquid-vapor behavior in porous systems with quench disorder, such as aerogels, is of particular interest because it may provide an experimental test of which theoretical model best describes critical phenomena in confined fluids. Currently, there are two competing theoretical models—the Random Field Ising model and the "single-pore" model. The experimental efforts to verify the validity of the models for confined binary liquid solutions have been obscured by experimental complications caused by the local composition gradients in pores as well as sluggish kinetics in the liquid-liquid region. SANS is particularly well suited to study the critical phenomena in small pores due to a short wavelength of neutron radiation (~ several Å), which allows for extracting information on the correlation length of the order of a nanometer and higher. In our experiments, silica aerogel (~96% porosity) was filled with CO_2 at different temperatures and pressures appropriate for bracketing the critical region. SANS measurements (Fig. 3) of the correlation length of the density fluctuations ξ indicate that quench disorder works to suppress density fluctuations in the critical region. The correlation length does not exceed the characteristic pore size which provides strong evidence in favor of the single-pore model.

Molecular-Based Simulation Techniques have been used to assess the behavior of water and water + CO_2 mixtures confined in a number of different nanoporous media (e.g., slit carbon, carbon nanotubes and mica). Experimental information determined from characterization of the porous media, adsorption-desorption isotherms, and scattering and spectroscopic assessments of fluids at different length and time scales provide crucial synergistic input to these simulations. The grand canonical Monte Carlo method (GCMC) was used to simulate water (SPC/E) in carbon-slit pores with widths of 0.6, 0.8, 1.0 and 1.6 nm and in (12:12; 20:20) single-walled carbon nanotubes with diameters of 1.36, 1.63, and 2.7 nm in the temperature range 298–600 K. A comparison of experimental sorption results (Fig. 2) and the

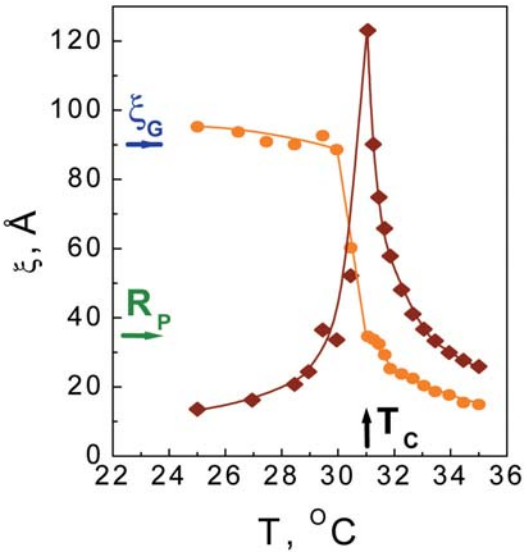

Fig. 3. Correlation length of density fluctuations of CO_2 for bulk (♦) and confinement (●). R_p = pore radius, ξ_G = aerogel correlation length, T_c = critical temperature.

simulations (Fig. 4) indicates that because of a competition between strong water-water and weak water-carbon interactions, adsorption isotherms are characterized by negligible uptake at low pressures, by pore filling following a capillary-like condensation mechanism, and by adsorption/desorption hysteresis loops. As temperature increases, the relative pressure at which pore filling occurs increases and the size of the hysteresis loops decreases. Differences between simulated and experimental results are primarily due to heterogeneous chemical composition (O, H in C fibers), pore connectivity, and non-uniform pore-size distribution, which are not accounted for in the simulation models.

Molecular dynamics (MD) simulations of water (TIP-4P) confined between two muscovite mica (2M1) surfaces focused on the hydration player structure and friction dynamics (Fig. 5). We investigated the hydration layer structure at the mica (001)-water interface. Under ambient conditions, for the "thick" water film (>1.0nm), we determined that the density oscillation of water oxygen as a function of distance *z* from the mean surface oxygen position of mica is only within 6 Å, roughly two water layers. When the confinement is below 1.0 nm, we also observed the adsorbed and hydration peaks of water molecules adjacent to the mica surface, similar to X-ray reflectivity experiments. Shearing of water films in MD regime showed that the hydrated potassium ions remains attached to the mica surfaces, and there were no significant stick-slips. The shear viscosity is found to be only 2–4 times that of the bulk values. This phenomenon suggests that the bound water molecules retain shear fluidity properties even at extreme confinement

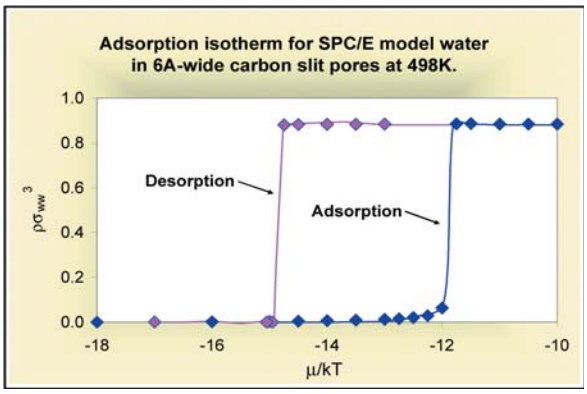

Fig. 4. GCMC results for water in slit-carbon pores. $\rho\sigma^3_{ww}$ is the reduced water density; μ/kT is the chemical potential ≅ p/p_o.

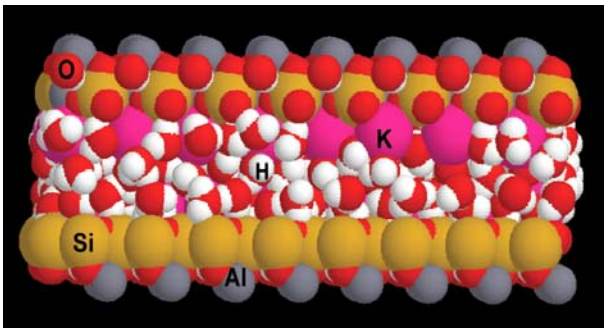

Fig. 5. 384 water molecules confined between two mica surfaces with a 0.96-nm separation.

Summary and Conclusions

A multidisciplinary, multi-institutional effort has addressed a number of key issues relevant to fluid-matrix interactions under confinement. Contributions have been made in the characterization of numerous complex nanoporous solid (e.g., porous silica, activated carbon fibers, zeolites) using a variety of techniques including TEM and small-angle X-ray and neutron scattering. Advanced sorption, scattering, and spectroscopic methods have documented fluid-fluid and fluid-matrix interactions of water, organic solvents such as chloroform, and CO_2 in confined geometries. MD simulations have provided the theoretical underpinning of the experimental results, particularly the water sorption isotherms.

Our new results on the structure and dynamics of fluids confined in porous materials at the nanoscale have broad relevance to DOE missions in Materials Sciences and Chemical Sciences, Geosciences and Biosciences (CSGB) within the Office of Basic Energy Sciences. An understanding of fluid behavior under confinement has broad application to problems related to catalysis, chemical separations, materials synthesis and durability, and environmental remediation. The effort also contributes to an understanding of fluid-solid interactions and corrosion relevant to the disposal of both civilian and defense-derived high level radioactive waste.

This project has already benefited the laboratory in several ways. Two BES renewal proposals to CSGB have been funded that redirected significant portions of their efforts to addressing issues of fluid confinement and associated reactivity in both experimental and natural mineralogical systems. Results obtained in this project were pivotal in helping establish the credibility needed to successfully defend the new directions taken in these proposals. Contributions realized from this project were instrumental in forming a vital part of the foundation upon which we developed a Research Focus Area (RFA) titled "Nanoconfined and Nanostructured Fluids" for the Center for Nanophase Materials Science (CNMS). Finally, results from this project along with the team we have assembled provide the necessary ingredients that will allow us future proposal opportunities in areas such as catalysis and hydrogen storage.

Publications Derived from This Project

D. R. Cole et al., "Influence of nanoscale porosity fluids behavior," *Proceedings of the 11th International Symposium on Water-Rock Interaction* (to be published).

Y. B. Melnichenko et al., "Density fluctuations near the liquid-gas critical point of a confined fluid," *Phys. Rev. Lett.* (submitted).

Y. B. Melnichenko et al., "Liquid-gas critical phenomena under confinement: small-angle neutron scattering studies of CO_2 in aerogel," *J. Molec. Liquids* (to be published).

J. L. Rivera et al., "Layering behavior and axial phase equilibria of pure water and water + carbon dioxide inside single carbon nanotubes," *Nano Letters* **2**, 1427 (2002).

M. Schilling and W. T. Cooper, "Effects of chemical treatments on the quality and quantitative reliability of solid state ^{13}C NMR spectroscopy of mineral soils," *Analytica Chimica Acta* (to be published).

M. Schilling and W. T. Cooper, "Identification of copper binding sites in soil organic matter through chemical modification and ^{13}C CP-MAS NMR spectroscopy," *Org. Geochem.* (submitted).

A. Striolo et al., "Water adsorption in carbon-slit nanopores," *Langmuir* **19**, 8583 (2003).

A. Striolo et al., "Simulated water adsorption isotherms in carbon nanopores," *Molec. Phys.* (submitted).

A. Striolo et al., "Temperature effect on water adsorption in porous carbons," *Fluid Phase Equilibria* (submitted).

Self-Organizing Polymers as Biomaterials

P. F. Britt,[1] J. W. Mays,[1,2] J. Pickel,[1] I. D. Chung,[2] and M. Liu[2]
[1]*Chemical Sciences Division*
[2]*Department of Chemistry, University of Tennessee, Knoxville*

This proposal seeks to create a new capability at ORNL in the design, synthesis, and characterization of polymeric materials, especially biomolecular materials, with novel properties. Because of the opportunities that exist for research into novel materials that mimic the properties and function of biological materials, this research project is focused on the synthesis, self-assembly, and characterization of amphiphilic block copolymers as biomaterials. Specifically, block copolymers that form micelles and vesicles are of interest because of their ability to compartmentalize additives into different domains and to be environmentally responsive. In this project, three different synthetic targets (block copolymers) were pursued utilizing living anionic and atom transfer radical polymerization techniques.

One of the greatest technical challenges facing chemistry, physics, and materials science today is the controlled synthesis of mesoscopic materials with well-defined properties, and assembly of these materials into macroscopic functional devices. One approach to address this grand challenge involves the synthesis and self-assembly of block copolymers to generate complex architectures with tailored mechanical, optical, electrical, or other physical properties. Block copolymers can be prepared by controlled/living polymerization methods with a high degree of control over the molecular architecture, which in turn controls molecular properties and function. This proposal seeks to create a new capability at ORNL in the design, synthesis, and characterization of polymeric materials, especially biomolecular materials, with novel properties. Because of the opportunities that exist for research into materials that mimic the properties and function of biological materials, this research project is focused on the synthesis, self-assembly, and characterization of amphiphilic block copolymers as biomaterials. Specifically, block copolymers that form micelles and vesicles are particularly interesting because of their ability to compartmentalize additives into different domains and to be environmentally responsive.

Three different synthetic targets were pursued in parallel using living anionic and controlled radical polymerization techniques. First, living anionic polymerization techniques were used to make linear block copolymers of styrene and ethylene oxide (PS-PEO) and mixed-arm star polymers of PS-$(PEO)_2$ to investigate the impact of molecular architecture (i.e., branching) on the self-assembly and biocompatibility of these materials. Attempts to prepare PS-$(PEO)_2$ by reacting living PS with excess CH_3SiCl_3, followed by removal of excess chlorosilane, and addition of living PEO were unsuccessful. Thus, a new synthetic approach was designed in which the hydroxyethyl terminated PS was coupled to 2,2-bis(phenyldioxymethyl) propionic acid. Deprotection by hydrogenolysis afforded the bis(hydroxymethyl) groups, which can serve as the initiation points for the polymerization of ethylene oxide to make PS-$(PEO)_2$ and potentially PS-$(PEO)_4$.

Second, block copolymers of substituted polystyrenes and acrylic acid were prepared by atom transfer radical polymerization methods (ATRP) to determine how the structure of the core influences the formation and stability of the polymer aggregates in solution, and how this impacts the encapsulation and release of hydrophobic substrates. Homopolymers of styrene (PS) and *t*-butyl acrylate (PtBA) were initially prepared by ATPR with narrow molecular weight distributions (M_w/M_n ca. 1.10) and controlled molecular weights (M_n = 5–10K). These macroinitiators were used to prepare block copolymers of PS-PtBA and polystyrene-polyacrylic acid (PS-PAA) after hydrolysis of the *t*-butyl group. In aqueous solution, PS-PAA formed spherical micelles and rods. The ATRP of substituted styrenes, including 4-*n*-butylstyrene and 4-*t*-butylstyrene, with *t*-butyl acrylate will be investigated next to determine the role of substituents in the aggregation of the polymers in aqueous solution (after hydrolysis of the *t*-butyl group) and the impact of the glass transition temperature of the micelle core on the release of hydrophobic substrates.

Finally, acryloyl amino acid derivatives were polymerized by ATRP in water to determine if the controllable properties of synthetic polymers could be combined with the exceptional functionality, activity, and

specificity of biological macromolecules. Monomers were synthesized by the reaction of β-alanine or phenylalanine with acryloyl chloride. Polymerization of acryloyl β-alanine (ABA) in water was surprising fast at room temperature, and polymers with M_n = 5, 8, and 12K were prepared in 70–87% yield. To provide better control of the block length of the poly(amino acids) and improve the copolymerization with other monomers, the impact of catalyst, inhibitors, initiators, solvent, temperature, and acid protecting groups are under investigation. Once polymerization conditions have been optimized, block copolymers will be prepared with poly(*N*-isopropylacrylamide), and the thermoresponsive behavior of the copolymers in aqueous solution will be investigated.

Advanced Ion Trap Mass Spectrometry for the Rapid and Confident Identification of Biological Agents

M. B. Wise,[1] K. J. Hart,[1] D. E. Goeringer,[1] L. J. Hauser,[2] I. F. Robbins,[3] and D. A. Clayton[4]
[1]*Chemical Sciences Division*
[2]*Life Sciences Division*
[3]*Computational Sciences and Engineering Division*
[4]*Engineering Science and Technology Division*

This proposal responds to the need for the rapid detection and positive identification of biological threat agents, including bacteria, toxins, and viruses, in complex environments. Because the protein component will most likely be differentiating for all types of biological agents, computational methods will identify and assess the efficacy of using biomarker proteins that are characteristic of and exclusive to the targeted biological agents. Employing an array of modern mass spectrometric techniques for their determination, the amino acid sequence(s) and molecular weight(s) then will be evaluated as an interrogation probe for the biomarker(s). Based on our findings, we will develop a concept for a biological agent mass spectrometer, produce a laboratory prototype instrument, and demonstrate its capabilities using a limited number of gamma-killed biological agents, toxins, and simulants.

The goals of this project are to develop novel mass spectrometry–based methodologies and portable instrumentation for rapidly detecting and confidently identifying low levels of biological agents including bacteria, toxins, and viruses.

The combination of analytical speed, sensitivity, and versatility offered by mass spectrometry (MS), especially when electrodynamic analyzers are employed, is virtually unmatched by any other single analytical technique. Consequently, a multi-step approach centered on MS is being pursued in developing an advanced strategy for the detection of biological agents. Computational simulations are being used to determine the applicability of protein biomarker analysis, within the context of MS, for differentiation and identification of specific biological threat agents. Experimentally, the actual detection and identification of a target organism within a complex mixture of other organisms is being assessed with simulations based on MS. In the instrumentation development area, our strategy is to incorporate proven MS technologies for biological agent detection while simultaneously considering novel scientific and engineering approaches. Thus, the proposed measurement approach is based on application of electrospray (ES) ionization for ion production, ion/ion reaction and dissociation of the mass-selected biomarker ions, and mass-to-charge analysis of the diagnostic fragment ions using electrodynamic devices.

Computational simulations compared a subset of 376 abundant genes from a target organism (*E. coli*) against a complex background mixture database containing ~80,000 unique entries from twelve microbial organisms. The purpose was to assess both the tryptic peptide level (bottom-up) and the whole protein level (top-down) ES-MS approaches for protein analysis as well as to determine the mass accuracy needed to make confident identifications. Results indicated that it is likely possible to identify a target organism within a complex background mixture using protein biomarkers while avoiding false positive identification. Furthermore, the simulations indicated that the top-down approach would be more viable for biothreat detection and identification as compared with the bottom-up method due to reduction in complexity of the database analysis, provided that ten fragments or more are produced per protein and that the mass measurement accuracy is at least ±10 Da.

Experimental simulations of the ES-MS detection and identification of a target organism (*E. coli*) within a complex mixture of four other organisms assessed the bottom-up technique under two scenarios: a "battlefield" scenario, in which threats are present at high concentration and rapid detection and identification is essential, and a "homeland security" scenario, in which threats are present at a considerably lower level and detection and identification is not as time sensitive. In the battlefield scenario, each simulation reported definitive detection of the target by returning multiple (>20) target peptides. The minimum ES-MS analysis time tested, 85 minutes, resulted in the identification of 21 target peptides, with only 7 false positive peptides. In the homeland security scenario, the target organism was present at varying dilution levels with respect to background: 1:1, 1:4, 1:40, 1:250, and 1:400.

The presence of the target was detected with relative certainty at the 1:1 (average of 267.3 peptide matches versus 7 false positive peptide identifications) and 1:4 (average of 83.3 peptide matches compared with 5 false positive peptide identifications) levels. For experimental simulations performed below these levels of the target organism, it could not be definitively stated that the target organism was present.

We have also completed the conceptual design of a mass spectrometer and associated operational method that promises to be particularly well suited for rapid and sensitive identification and analysis of protein biomarkers. The concept consists of a tandem configuration of a three-dimensional RF quadrupole ion trap, a linear RF quadrupole, and a time-of-flight mass spectrometer, along with the associated method of operation whereby the combination generates a complete three-dimensional mass spectrum of parent and product ions on a time scale that is significantly faster than current commercial mass spectrometers. Fabrication and evaluation of such a prototype instrument is currently in progress.

As indicated in the original proposal, we anticipate that this project will result in instrumentation and techniques that will give ORNL a technological advantage in the area of biological agent detection. More specifically, the MS-based detection and identification system will surpass the capabilities of other analytical technologies such as polymerase chain reaction and immunoassay with regard to the range of biological agents that may be detected. We also believe that by being able to detect changes in the basic structure of key proteins, this approach may be less vulnerable to being thwarted by genetic engineering of the biological agents. The DoD, DHS and other agencies should be very interested in this technology as the basis for their next-generation biodetectors/identifiers.